Check for
updates

Effects of temperature on structural and linear/nonlinear optical properties of CdS nanoparticles film deposited by chemical reaction method

Harith A. Hasan[1] · Nadia A. Hussein Al-Assady[2] · Hussain A. Badran[3] · Raeed K. Alfahed[4] · Khalid I. Ajeel[3]

Abstract

The effect of annealing temperature on the structure and linear/non-linear optical properties of CdS-NPs was studied. The structural, optical properties and crystallite size were investigated using X-ray diffraction, Fourier Transform Infrared technique, ultraviolet–Visible absorption spectroscopy and scanning electron microscopy. The calculation shows that the CdS crystallized in cubic phase and formed NPs with average crystallite sizes of 17.2, 20.1 and 23.3 nm and the microstrain is about 0.034, 0.030 and 0.026, for CdS films annealed at 300 °C, 400 °C and 500 °C respectively. The non-linear refractive indices (n_2) of the CdS-NPs are determined using open and closed Z-scan techniques. The optical limiting (OL) behaviors have been also investigated. It has been shown that the OL efficiency depended on the CdS-NPs temperature. Under laser irradiation, self-diffraction rings were seen in CdS-NPs-300 °C, CdS-NPs 400 °C, and CdS-NPs 500 °C as increased input power, each pattern is created by a rise in the number of rings and the diameter of the outermost rings. The assessment of the figure of merit (W > 1) and thermal figure of merit demonstrates that, the CdS-NPs films are highly sufficient for use in nano-optical technology. The potential of CdS-NPs can be used in photonic and holographic devices as shown by this studying. The aim of the present study is to find fresh applications for CdS-NPs in the world of optical modulators.

Keywords CdS-NPs · Optical properties · Energy band gap · Figure of merit · Extinction coefficient

1 Introduction

The nanoparticle materials of II–VI group semiconductors have received considerable attention recently according to the manifestation of new physical phenomena with potential for future device applications (Althobaiti et al. 2022a, b; Ali et al. 2022a, b). Low-dimensional semiconductors have novel properties that offer new ideas in excellent technological

✉ Hussain A. Badran
   hussain_badran@yahoo.com

Extended author information available on the last page of the article

characteristics such as optoelectronics, electrical, magnetic, dielectric, and piezoelectric properties, since NPs have a greater number of surface atoms than bulk materials, (Lee 2005; Manickathai et al. 2008; Srinivasa et al. 2011; Mahdi et al. 2012; Ali 2021). In our knowledge, the buffer materials must meet the parameters of a perfect band gap, excellent transmittance, and low series resistance (Lee et al.2009; Lazim et al. 2015; Cheng et al. 2018; Hussain et al. 2018; Ajeel and Kareem 2019; Tezuka et al. 2011). Cadmium sulfide (CdS) nanostructure is one of the widely studied material due to it's expected gap emission lies very close to the highest sensitivity of human eyes. Thus it could be assumed that CdS nanostructure films are an appealing host of photonic systems (Qi et al. 1996; Ullrich et al. 2000; Chikan 2011).

CdS-NPs are n-type semiconductors and possess unique optical properties such as the high absorption band makes these materials useful for applications in photonic and photoelectric devices as photo-resistance sensors, low-cost solar cells for energy conversion, field effect transistors, laser components, optical waveguides, light-emitting diodes, non-linear optical apparatus and biological sensors (Kale and Lokhand 2005; He et al. 2011; Mahawela et al. 2005; Badran et al. 2016a, b). Hussain et al. (2021) CdS-NPs with wide direct band gap semiconductor was used with CdTe and Cu (In,Ga) Se$_2$ semiconductors to fabricate photovoltaic cells given its optimum band energy of 2.42 eV for optical windows (Ziadan et al. 2012; Fedyaeva et al. 2016; Althobaiti et al. 2022a, b) in general CdS thin films have high resistance and optical transmittance, both of which may be created by the deposition process. The heat treatment and structural changes are the fundamental steps to influence the optoelectronics properties of CdS-NPs films and hence the devices. Thin films of transparent conducting oxides (TCOs) have gained a lot of significance because of their possible applications in photovoltaic and 3 optoelectronic devices. Among the TCOs, CdS nanocrystalline thin films have lately gained popularity due to their distinct physical, chemical, and mechanical characteristics when compared to their bulk counterpart. They are widely employed in optoelectronic devices because of the variation in particle size tunes emission in the visible area of the electromagnetic spectrum. Because CdS thin films have strong photosensitive characteristics, they can be used to make thin film transistors, light detectors, and solar cells. By manipulating the size, structure, and surface states of nanocrystalline materials, fundamental characteristics of semiconducting material, such as optical, electrical, and magnetic capabilities, may be controlled (Alaa and Ahmed 2021; Ahmed 2016).

Many methods have been used to synthesis compound semiconductor (ZnO, CdO, CdSe, ZnSe, ZnS and CdS) from aqueous solutions such as sol–gel method microwave heating chemical bath deposition (CBD) based on the slow release of cadmium ions and sulfide ions in an aqueous alkaline bath and the subsequent condensation of these ions on substrates suitably mounted in the bath and spin coating method, etc. (Ramteke and Lanje 2017; Ramteke et al. 2018; Mahesh et al. 2020).

In this work, we provide a novel approach to the synthesis of CdS nanoparticles using a polymer-assisted chemical reaction process. Cadmium sulfide nanoparticles)CdS-NPs(deposited on glass substrates using a simple chemical reaction method (CRM) and annealed at different temperatures, 300 °C, 400 °C and 500 °C. According to the literature that is currently available, there are just a few papers on the polymer-assisted production of CdS nanocrystals. The creation of films containing cadmium sulfide nanoparticles were analyzed using Z-Scan while the temperature maintained around 300 °C and 500 °C. Regarding various temperatures, the CdS-NPs exhibit good optical limiting characteristics. Under 532 nm cw laser irradiation, self-diffraction rings (spatial self-phase modulation (SSPM)) were seen in CdS-NPs-300 °C, CdS-NPs-400 °C, and CdS-NPs-500 °C. With

increased input power, each SSPM is created by a rise both in terms of the quantity of rings and the size of the outermost ring. The purpose of the present study is to find fresh applications for CdS-NPs in the world of optical modulators.

2 Materials and methods

All chemical materials used in this procedure were supplied by sigma Aldrich. CdS-NPs films were prepared using a chemical reaction method. The aqueous solution was prepared by dissolving Polyethylene glycol (PEG) in 100 ml of deionized water. A few amounts (0.2 ml) of the prepared mixture were then dissolved in 5 ml of 2-methoxyethano for 60 min. Then, 0.15 M of $Cd(CH_3CO_2)_2$ $2H_2O$ (Molecular Weight 266.53) was added to the mixture. The prepared solution number (A) of PEG/ 2-methoxyethano/ water/Cd $(CH_3CO_2)_2 \cdot 2H_2O$ was left for 60 min. Separately, another solution number (B) was made by dissolving 0.15 M of Thiourea CH_4N_2S (Molecular Weight 76.12) in 5 ml of 2-methoxyethano for 30 min. Solution (A) was then added dropwise to solution (B) and the obtained mixture was left for a few hours in ambient condition. The glass slide substrates were washed with deionized water and then cleaned ultrasonically for several minutes in acetone, and ethanol to remove any remaining dust and/or dirt. The prepared solution was deposited on the glass substrates using the spin coating technique for 1000 rpm for 30 min. The deposition process was achieved to obtain an optimum thickness of 97.9 nm. The spin coated step was followed by annealing process on a hot plate a temperature of 300, 400 and 500 °C for 45 min. The obtained samples are denoted in this paper as CdS-NPs-300, CdS-NPs-400 and CdS-NPs-500 respectively. The chemical preparation steps are displayed as shown in Fig. 1. The fabricated films were examined through various techniques such as scanning electron microscopy (FEI Quanta 600 environmental), X-ray diffractometer (XRD) (Philips, EMPYREAN), FTIR (IRPRESTIGE 2), UV–Vis Spectrometer (Lambda 750S 60 mm Sphere) and Ellipsometry spectroscopic (M-2000 Woolam).

3 Results and discussion

3.1 Structural analysis

The investigation of these samples by X-ray diffraction (XRD) is a basic approach to identify CdS-NPs and know the nanostructural and crystalline features. This sample is also being developed for use in a variety of scientific and practical sectors, thus the development of this material is important. (Abdolhossein et al. 2022; Alaa et al. 2020). The X-ray diffraction (XRD) patterns of annealed CdS-NPs films at 300 °C, 400 °C, and 500 °C respectively are shown in Fig. 2. It can be seen, the XRD of CdS-NPs reveals that the peak intensity varies with the annealing temperatures, indicating that the film's structure will change. By comparing with the standard data, the type of the film has a particular hexagonal phase which has only one peak for un-annealed film (Manickathai et al. 2008). The film which annealed at 400 °C has four strong sharpener diffraction peaks, while there are five peaks visible in the XRD pattern of the CdS film annealed at 500 °C relating to the hexagonal plane than the film annealed at 300 °C which is indicated that the temperature was improved crystallinity of the films (Badran et al. 2017; Hussain et al. 2021; Ziadan et al. 2012; Fedyaeva et al. 2016). The main peaks
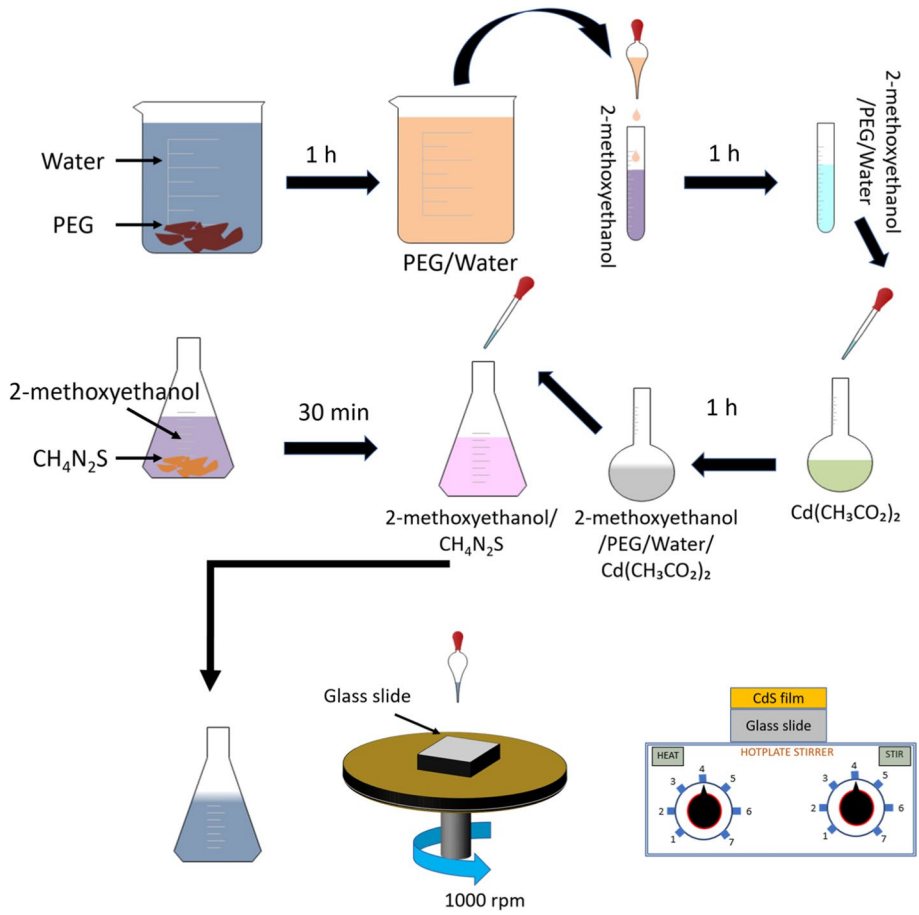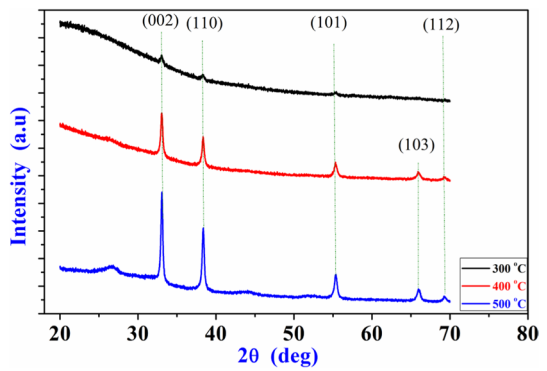
Fig. 1 Schematic illustration of the procedure for the synthesis of CdSNPs films

Fig. 2 XRD pattern for CdS-NPs film

at $2\theta = 26.11°$, $33.13°$, $38.5°$, $55.26°$, and $66°$ of CdS samples correspond to the (002), (110), (101), (103) and (112) planes of CdS, respectively. It can be noticed from Fig. 2 that there are overlapped by the peaks of the two samples, 400 °C and 500 °C of hexagonal CdS (Gutierrez et al. 2015; Hussain et al. 2021; Aziz et al. 2017; Rathore et al. 2017). The improved crystallinity of the films and larger crystalline sizes that occurred as the annealing temperatures increased may be attributed for these results.

The lattice parameters a and c can be determined from the XRD line position according to the following relation (Kathirvel el al. 2009; Alaa et al.2021):

$$\frac{1}{d_{hkl}} = \frac{4h^2 + hk + k^2}{3a^2} + \frac{l^2}{c^2} \tag{1}$$

where d_{hkl} is the interplaner spacing and hkl are the Miller indices. For pure CdS film $a = 4.127A°$ and $c = 6.6112A°$ while the lattice parameters decrease with annealing temperature to $a = 4.12A°$ and $c = 6.59A°$. The mean crystallite size (D) of the films can be determined by using Scherrer's formula (Lazim et al. 2015; Kathirvel el al. 2009):

$$D = \frac{0.9\lambda}{\beta \cos\theta} \tag{2}$$

where λ is the X-ray wavelength is equal to be $1.5406A°$ and β represents the full width at half maximum (FWHM) of the film diffraction peak at 2θ, where θ is the Bragg diffraction angle. The average grain sizes determined are shown in Table 1. A dislocation is a crystallographic defect, or irregularity within a crystal structure. The presence of dislocation (δ) strongly effects a lot of characteristics of materials. The dislocation density was estimated from the following relation (Kathirvel el al. 2009; Ali et al. 2021):

Table 1 Effect of annealing temperature on the structure parameters of CdS-NPs films

$2\theta)$deg(	hkl	Annealing temperature (°C)	Crystallite size D(nm)	δ Lines/ $m^2 \times 10^{15}$	$\varepsilon \times 10^{-3}$
26.11	(002)	300	–	–	–
		400	–	–	–
		500	21.6	33.8	26.1
33.13	(110)	300	16.5	58.3	34.6
		400	18.8	44.6	30.2
		500	22.1	32.8	25.9
38.5	(101)	300	16.8	56.5	34.4
		400	19.2	43.3	30.1
		500	23.3	31.8	25.8
55.26	(103)	300	18.2	33.9	33.9
		400	20.4	29.7	29.7
		500	24.2	25.4	25.4
66	(112)	300	–	–	–
		400	21.6	34.1	29.3
		500	25.4	25.1	25.1

$$\delta = \frac{1}{D^2} \tag{3}$$

The average micro strain (ε) of prepared films were also determined using Stokes-Wilson relation given by (Ali et al. 2022a, b; Ahmed and El-Radaf 2023):

$$\varepsilon = \frac{\beta}{4 \tan \theta} \tag{4}$$

The structure parameters of CdS-NPs films are shown in Table 1. It can be observed from Table 1, that the increase in crystallite size with increasing annealing temperature, this rise may be linked to an increase in the crystallinity of the CdS-NPs films, which has seen a degree of crystallinity of the films improvement recently. The crystallinity is highly related to FWHM value.

The Scherrer's formula gives a rough estimate of crystallite size and the micro strain (ε) can be neglected. Therefore the average micro strain (ε) and mean crystallite size (D), both of which are contributors to the line broadening shown in the XRD patterns can be determined by using the Williamson–Hall (WL-H) Plotting method. The plotting depends on the 'FWHM' of the diffraction peak. The relation of WL-H plotting can be written as:

$$\frac{\beta \cos \theta}{\lambda} = \frac{k}{D} + \frac{4 \sin \theta}{\lambda} \tag{5}$$

A plot of $\beta \cos \theta$ against $\sin \theta$ will give a straight line while the mean crystallite size (D), and the average micro strain (ε) can be evaluated from the intercept and slope respectively. The average crystallite size is estimated to be average crystallite sizes of 17.2, 20.1 and 23.3 nm and the micro strain is about 0.034, 0.030 and 0.026, for CdS-NPs films annealed at 300 °C, 400 °C and 500 °C respectively by using the debye–scherrer relation. While by WL-H Plotting gave that the average particle size 17.1, 20 and 21.8 nm and micro strain (ε) is about 0.034, 0.03 and 0.026, respectively for CdS-NPs films annealed at 300 °C, 400 °C and 500 °C. Figure 3 illustrates how the grain size increases as the annealing temperature rises, this rise in quality is likely responsible for the improvement shown in the CdS-NPs films.

Fig. 3 Variation of the average crystallite size (D) and micro-strain (ε) as a function of temperature
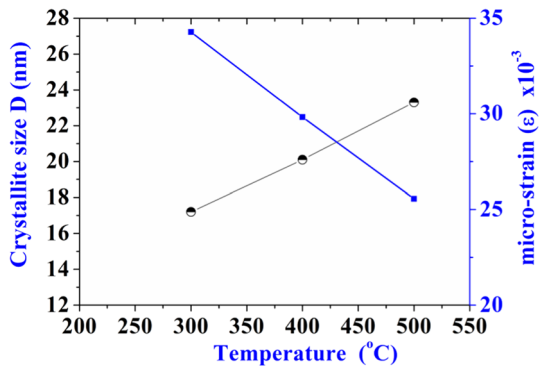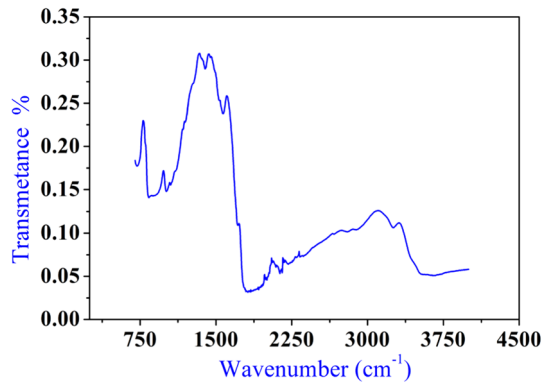
Fig. 4 FTIR spectra of CdS film

3.2 Fourier Transform Infrared (FT-IR) spectrum

The FTIR spectra of the cadmium sulfide films are shown in Fig. 4. The Fourier Transform Infrared technique was used to characterize the different bonding arrangement in the CdS. The spectra show that the strong absorption band located around 702 cm^{-1} corresponds to the Cd–Stretching band. There are weak absorption bands located around ~ 820 to 957 cm^{-1} and around ~ 1306 to 1527 cm^{-1} which correspond to the C–C and S=O stretching band respectively. It can be observed from the figure that the absorption peaks centered at 3165 and 3525 cm^{-1} which to be specified to the O–H stretching of the CdS films.

3.3 Scanning electron microscopy images (SEM)

The investigation of surface morphology and the uniform dispersion of the films result in desired features that may be put to use in a variety of optoelectronic applications. This includes the employment in solar cells and other electronic devices, as well as its use in the production of small and giant television displays and optical switch devices. The SEM images of CdS-NPs films were illustrated in Fig. 5. It was shown that the roughness of the CdS-NPs films surfaces is relatively low, and when the particle sizes of the films were increased, a smooth surface was generated. Furthermore, the surfaces did not exhibit any pinholes or porosity and this agreed with results of the X-ray diffraction. The films showed an improved surface that had a very low degree of distortion (Bokka et al. 2016). It can be noticed from the image morphology of CdS, which the particles are in the nanometer range. Figure 5 shows with two magnifications that the grains have combined to form clusters (Mahdi et al. 2009).

4 Optical analysis

The optical constants of CdS-NPs films deposited on glass substrates were determined from absorbance *A* and the transmittance *T* spectra were registered over the wavelength range 300–800 nm using the UV–Vis spectrophotometer. Figure 6 depicted the absorption spectra and average absorption of deposited CdS-NPs films and annealed at temperatures of 300 °C, 400 °C, and 500 °C respectively. The figure clearly shows that the absorption
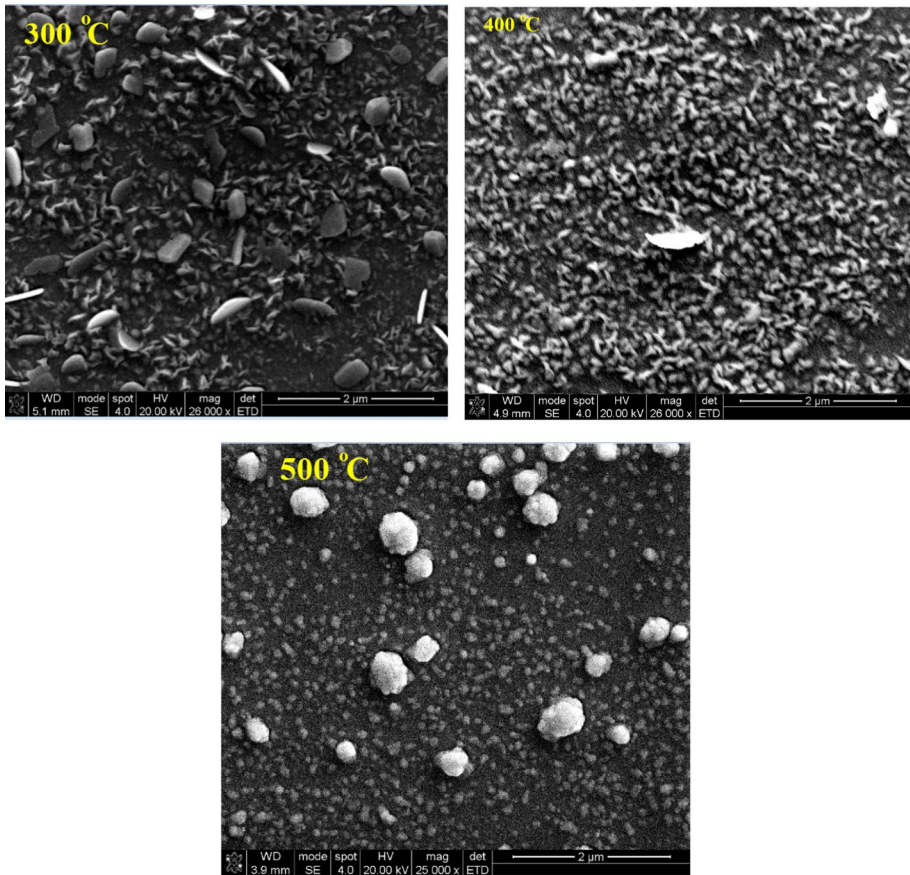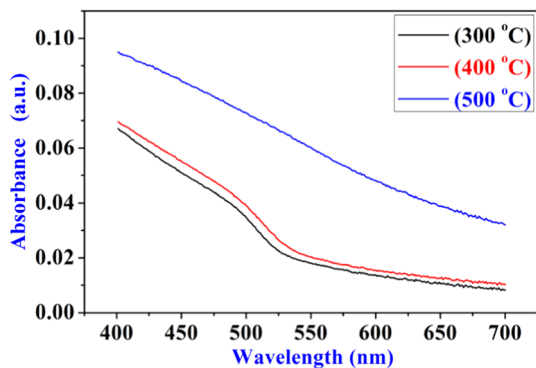
Fig. 5 SEM of CdS-NPs film under increasing annealing temperatures degree from top to bottom

Fig. 6 UV–Visible absorbance spectra of CdS-NPs

spectra for all CdS-NPs films declined as the wavelength increased while the transmittance intensity increased with increasing wavelength in the visible region as shown in Fig. 7 to reach a maximum value of 97% at annealing temperature of 400 ^{o}C which might be

Fig. 7 Transmittance spectra of CdS-NPs
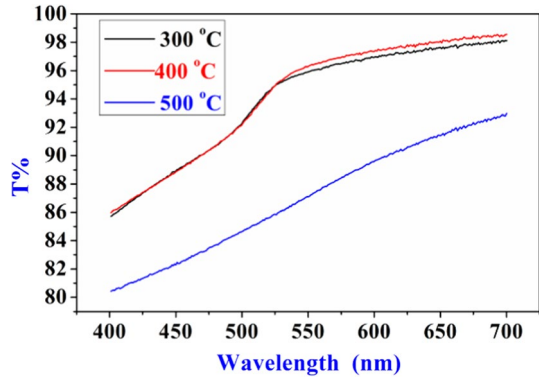
attributed to the absorption of light and development of micro—crystallites as well as the reason for this behavior is that the annealing leads to decrease the localized state density which rises the transmittance values. This result is agreement with that reported by other researchers (Pantoja 2013). In order to get the best growing conditions for the CdS-NPs to be utilized as a buffer layer or window layer for solar cells varistor, luminescent material as well as electro acoustic wave device, it is crucial to consider their optical qualities.

The extinction coefficient k of the film was determined from the relation (Ahmed 2022):

$$k = \frac{\alpha_{Ab}\lambda}{4\pi} \tag{6}$$

where α_{Ab} is the absorption coefficient. The refractive index is a fundamental optical property of nanostructures films, that is directly to the optical, electrical and magnetic properties, as well as it is interesting to investigate the physical and chemical of semiconductor by optical techniques (Yang et al. 2018). The refractive index (n) of CdS-NPs films were estimated from the absolute values of the absorbance and transmittance of the studying films, which is given as (Shinde et al. 2021):

$$n = \left(\frac{1+R}{1-R}\right) + \left[\frac{4R}{(1-R)^2} - k^2\right]^{1/2} \tag{7}$$

where R is the film reflectance. It is clear from the Fig. 8a, b that both of k and n show an increase in values with increasing the incident photon energy this is in accordance with the rise in the coefficient of absorption.

The real part (ε_r) and the imaginary part (ε_i) of the dielectric constants are related to n and k values and they determined by using the following relations (Saravanan1 et al. 2011; Ahmed and Ishu 2021);

$$\varepsilon_r = n^2 + k^2 \tag{8}$$

$$\varepsilon_i = 2nk \tag{9}$$

Figure 8 shows the dependence of ε_r and ε_i of dielectric constants on the incident photon energy hv for CdS-NPs annealed at temperatures of 300 °C, 400 °C, and 500 °C respectively. It can be observed from the figure that the ε_r depends on n because the effect of k is very small and that the ε_i depends on extinction coefficient. Also it can be seen from the figure that, the

Fig. 8 Extinction coefficient (k) and refractive index (n) as function of the incident $h\nu$
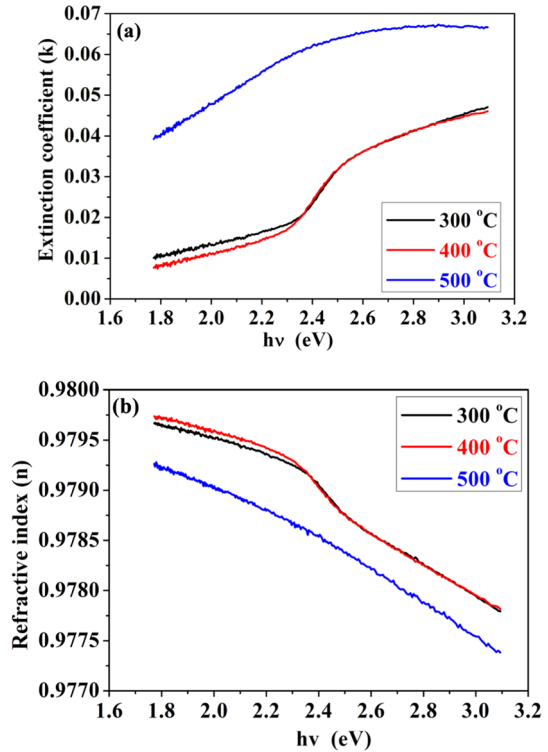
values of the ε_r are greater than the ε_i. Also it can be seen from the Fig. 9 that the values of ε_r and ε_i are decreasing with increases the incident photon energy.

The optical conductivity (σ_{op}) of the CdS-NPs film is related to the absorption coefficient (α) and the velocity of light according to the following relation (Pankove 1971; Moss 1974).

$$\sigma_{op} = \frac{\alpha nc}{4\pi} \tag{10}$$

where c is the velocity light. The variation between optical conductivity of CdS-NPs annealed at temperatures of 300 °C, 400 °C and 500 °C, respectively as a function of the photon energy ($h\nu$) can be depicted in Fig. 10. It is noticed from the figure that the optical conductivity (σ_{op}) is increasing with increases the photon energy ($h\nu$), this behavior is similar to the absorption coefficient since the optical conductivity depends on the absorption coefficient.

The optical energy band-gap (E_g) was estimated from the following relation (Eckertova 1986; Ali 2020):

$$(\alpha h\nu) = B(h\nu - E_g)^{n'} \tag{11}$$

where $h\nu$ is the incident photon energy, B is a constant depends on the transition probability, n' is an index depends on the kind of the electronic transition (Chikan 2011). For direct band gap $n' = 2$ this mean that the transition is direct allowed transition. The value of optical energy band gap (E_g) of CdS-NPs film can be estimated from Fig. 11 by plot of $(\alpha h\nu)^2$ against the incident photon energy, $h\nu$, and then plot the intersection of the linear

Fig. 9 Real (ε_r) and the imaginary (ε_i) dielectric constants as a function of $h\nu$
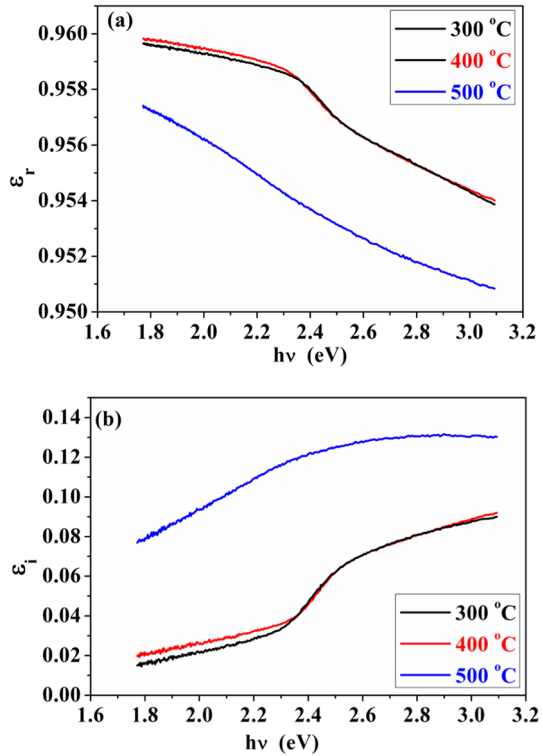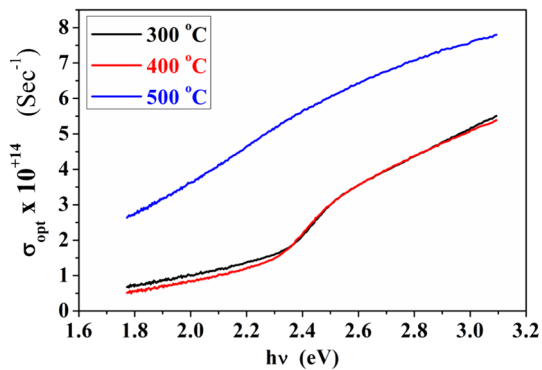

Fig. 10 Optical conductivity (σ_{op}) of the CdS-NPs film as a function of $h\nu$

part of the curve when the $(\alpha h\nu)^2 = 0$. The results showed the values of E_g are 2.49 eV and 2.42 eV for CdS-NPs film annealed at temperatures of 300 °C and 400 °C respectively. After annealing at 500 °C the film has an energy gap equal to 2.05 eV. This suggests that a lower band gap may be achieved by raising the annealing temperature for CdS-NPs films in accordance with a lower dislocation density and the temperature was improved crystallinity as well as increase in grain size on annealing of films. Such band gap depends on film crystallinty has been reported for CuInSe$_2$ and CuGaSe$_2$ polycrystalline thin films (Dresselhaus 1998).

Fig. 11 A plot of $(\alpha h\nu)^2$ as a function of hv for CdS-NPs films
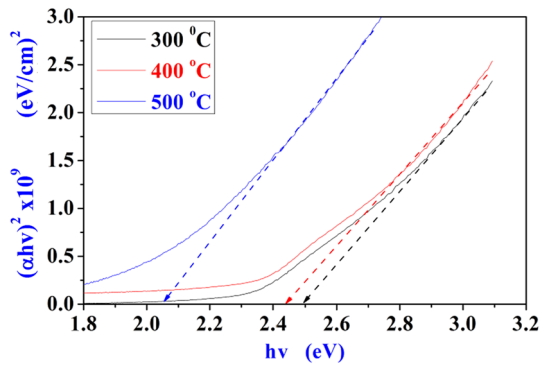
The factors and the method that effect the band gap are the dislocation density, crystalline phase change from cubic to hexagonal and CdS evaporation that causes the change in sample stoichiometry, oxidation as well as the degradation of the sample at annealing temperatures (Kadem et al. 2020; Chichibu 1998).

5 Nonlinear optical properties

5.1 Third order analysis

A radiationless process with a typical duration of millisecond transforms the absorbed light into heat when a light beam illuminates an absorbent substance. As a result of the medium's absorption of the light, its temperature increases, which changes its refractive index and results in self-diffraction (SFD) (Hussain et al. 2021). Temperature is one of the elements that have a role in determining the refractive index. The thermo-optical coefficient, which is represented by the parameter *dn/dT*, causes the refraction index to change $[\Delta n = (dn/dT)\Delta T]$ as the temperature is increased by T.

A single fundamental beam (Gaussian laser) in tight focus geometry was utilized to analyze the nonlinear medium's transmittance as a function of sample location relative to the lens' focal point. The Z-scan method was used to characterize the CdS-NPs nonlinear behavior, due to its ease of use and accurate method for calculating the thermal conductivity and the thermo-optical coefficient in both magnitude and sign, the single-beam Z-scan technique is appealing. In order to conduct the Z-scan studies, a laser with a wavelength of 532 nm (Solid state laser-532-100 T) and a beam with a diameter of 1.2 mm (1/e2) was used. The beam was focused by a positive lens (f = +100 mm focal length). It was determined that the laser beam's waist, ωo, at the focus was equal to 49.92 μm, which corresponds to the Rayleigh length ($Z_R = 14.7$ mm). At the focus, the greatest laser intensity that was incident was about 4.599 KW/cm^2.

The photo detector and Field Max digital power meter with two optical visible sensors were situated at far field to measure the transmittance of the CdS-NPs film as it moved along the focused beam's propagation direction (z). The experimental Z-scan arrangement was similar to the one described in (Badran 2015).

From the open aperture Z-scan data, the non-linear absorption coefficient (β) may be calculated according to the relation (Al-Salihi et al. 2020; Badran et al. 2017).

$$\beta = 2\sqrt{2}\Delta T / I_\circ L_{eff} \tag{12}$$

where ΔT is one valley transmittances at the open aperture Z-scan curve, $I_o = 2P/\pi\omega_o^2$ is the intensity of the laser beam at focus (z = 0). Also, Δn can be related to the total refractive index of the medium (n) and the back-ground refractive index) n) as (Ghosh et al. 2010; Al-Saymari et al. 2013):

$$n = n_\circ + \Delta n \tag{13}$$

In this case, the linear transmittance of the aperture S is represented by the equation $S = 1 - \exp(-r_a^2/\omega_a^2)$ (Ketam and Hussain 2012; Alfahed et al. 2020a, b), where r_a represents the radius of the aperture and ω_a represents the beam radius at the aperture while operating in the linear domain. By using the formula, we may establish a connection between the relative phase shift ($\Delta\phi_\circ$) and the third-order nonlinear refractive index (n_2) (Al-Hazam et al. 2019; Badran 2013; Hussain et al. 2016a, b);

$$\Delta\phi_\circ = k' n_2 L_{eff} I_\circ \tag{14}$$

where k' is the wave number ($k' = 2\pi/\lambda$), λ is the CW laser wavelength, $L_{eff} = (1 - \exp(-\alpha_{Ab}Th_S))/\alpha_{Ab}$ is the effective thickness of the CdS-NPs sample and Th_S is the thickness of the sample.

The data from the samples' film's closed-aperture Z-scan are displayed in Fig. 12. A high (peak) transmittance is shown on the normalized closed-aperture Z-scan curve, which is followed by a minimum (valley) transmittance. The peak-to-valley contour of the sample exhibited a negative nonlinear refraction, which is suggestive of an activity known as self-defocusing (SED) (Badran et al. 2012a, b). The local temperature-dependent fluctuation of the refractive index is the physical cause of the self-defocusing feature. The difference between the normalized peak and valley transmittances ($T_P - T_V$) can be referred to as the peak-valley normalized transmittance difference (T_{P-V}).

Figure 13 displays the normalized open aperture (OPA) z-scan curves for the various CdS films annealed at different temperatures. This figure makes it clear, when the sample is pushed toward the focus (from $-z$ to $+z$), the laser beam intensity lowers to attain its minimal value (z = 0) (valley position). This trend points to the possibility that the sample has reverse saturable absorption (RSA) and it also indicates that the nonlinear absorption coefficient (β) is positive.

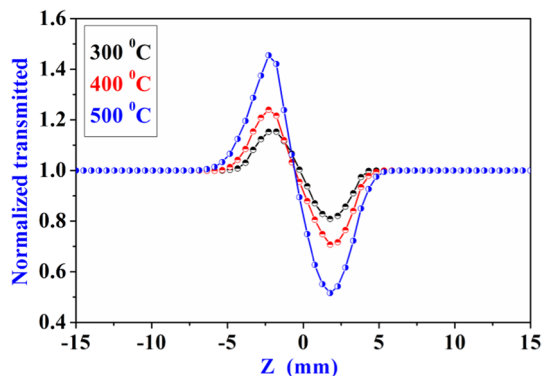**Fig. 12** Closed Z-scan data for CdS-NPs
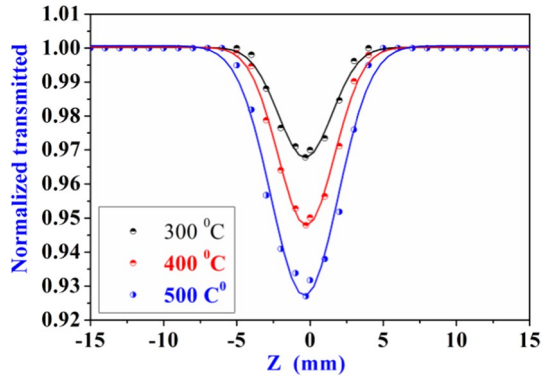
Fig. 13 Open aperture data for Cd-SNPs
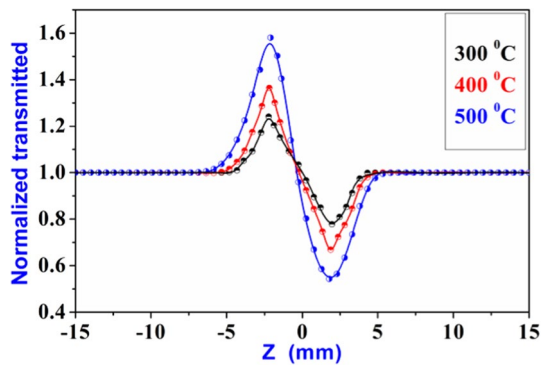

Fig. 14 Pure Z-scan data for CdS-NPs

Table 2 Figure of merit and nonlinear parameters for CdS-NPs films

CdS-NPs temperature (°C)	$\Delta n x 10^{-3}$	n_2 (cm^2/W) $\times 10^{-6}$	W
300	5.22	-11.35	1.03
400	7.64	-16.62	1.09
500	19.9	-43.42	1.25

If nonlinear absorption is present, as in our case, the pure non-linear refraction can be extracted by simply dividing the curves obtained from the two Z-scan modes (closed aperture (CLA) / OPA). The ratio of Figs. 12 and 13 scans are shown in Fig. 14. Data obtained in this manner solely reflects the effects of nonlinear refraction. Table 2 contains the computed β and n_2 values as well as the measurement data from Figs. 13 and 14, as well as utilizing Eqs. 12, 13, and 14. In order to assess the use of 2π phase shift in such devices, the figure of merit W must be met (Alfahed et al. 2020a, b):

$$W = \frac{\Delta n_{max}}{\alpha \lambda} > 1, \tag{15}$$

Table 2 provides the predicted value of the figure of merit for CdS-NPs films when excited at 532 nm, it shows that the nonlinear optical characteristics and figure of merit values of CdS-NPs samples are adequate for use in communications and optical switching devices. CdS-NPs show promise for usage in nonlinear optical systems due to their quick response time and significant nonlinear refraction. The value acquired from the Z-scan data can then be used to calculate the materials' thermally induced on-axis n_2 using the equation (Sheik-Bahae et al. 1989; Alfahed et al. 2021; Ogusu et al. 1996):

$$n_2 = \frac{dn}{dt} \frac{\alpha \omega_0^2}{4 k_{th}} \tag{16}$$

where dn/dT (K^{-1}) is the CdS-NPs films thermo-optic coefficient or the change in refractive index dn with temperature. k_{th} is the thermal conductivity (Badran 2014). Lastly, when the thermal conductivity ($k_{th} = 0.247$ W m^{-1} K^{-1}) is used with Eq. 16 the thermo-optic coefficient dn/dT of the CdS-NPs-300 °C, 400 °C and 500 °C has been found equal to -3.84×10^{-5} K^{-1}, -4.05×10^{-5} K^{-1} and -4.68×10^{-5} K^{-1}, respectively.

5.2 Self diffraction ring measurement

The experimental set-up, which is depicted in Fig. 15, included CdS-NPs. The identical light source that was used in the Z-scan experiment is being employed here. The irradiation laser light was focused onto each nano-particle sample using a glass lens with a + 100 mm focal length, and ring patterns were registered using a sensitive wide preacher digital camera. The relation can be used to determine the beam radius (ω) at the sample entrance (Ghorbani et al. 2016):

$$\omega = 1.22 f \lambda / \omega_0 \tag{17}$$

Equation 17 states that the beam's radius at the CdSNPs depends on λ. So that, for f = + 100 mm, $\lambda = 532$ nm and $\omega_0 = 1.3$ mm (at 1/e2) ω is equal to 49.92 μm. The Rayleigh limit (range), Z_R can be computed using the relation (Badran et al. 2016a, b), and it must be shorter than the CdS-NPs film thickness (Th_S) for the nonlinear thin medium conditions to be met.
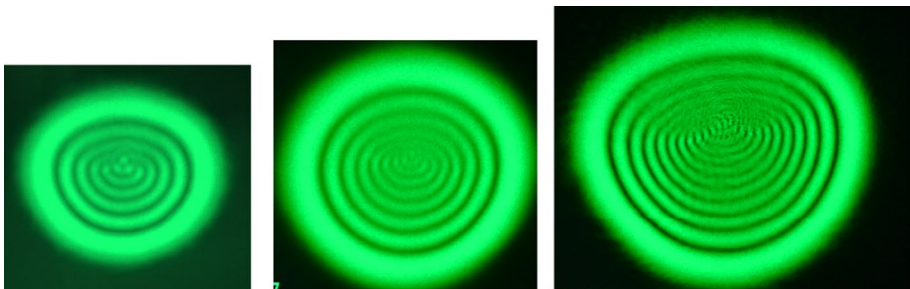

Fig. 15 2D intensity distributions of CdSNPs rings patterns caused by far field diffraction. **a** CdS-NPs-300 °C **b** CdS-NPs-400 °C **c** CdS-NPs-500 °C using laser power of 30 mW
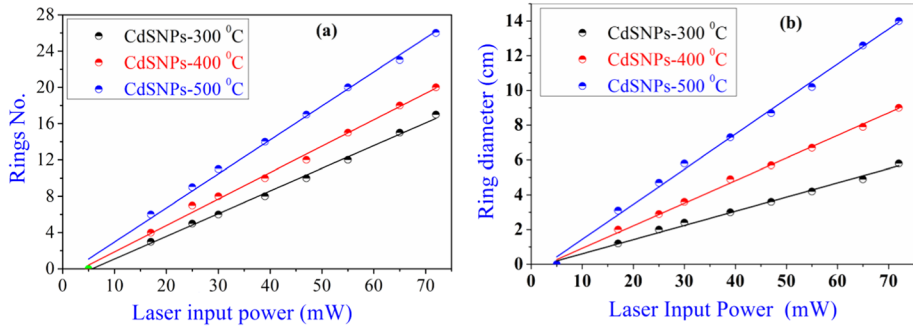
Fig. 16 a Rings Number, N, and **b** Outermost rings diameter for CdS-NPs-400 °C, CdS-NPs-400 °C and CdS-NPs-500 °C against laser input power respectively

$$Z = \frac{\pi \omega^2}{\lambda} \tag{18}$$

so that $Z_R = 14.71$ i.e., the CdSNPs film thickness criteria is satisfied ($Th_s < Z_R$). Figure 15 displays CdS findings for CdS-NPs films at the laser input power about 30 mW for the immediate post-irradiation diffraction ring patterns. The relationship between the number of rings (N) and annealed at various temperatures, 300 °C, 400 °C and 500 °C can be seen clearly in Fig. 15. i.e., as $\alpha_{Ab} = 94.88$ cm^{-1} for CdS-NPs-300 °C, N=6, for CdSNPs-400 °C, $\alpha_{Ab} = 131.73$ cm^{-1}, N=8, and for of the CdS-NPs-500 °C $\alpha_{Ab} = 297.54$ cm^{-1}, N=11. The growth in the number of rings may be affected by the absorption coefficient as well as by the different annealing temperatures.

Figure 16 plots the input power from each sample at a wavelength of 532 nm against the change in the number of rings and diameter of the outer-most ring in each self pattern. The diffraction ring pattern shows signs of self-defocusing when one moves from the middle of each design to the patterns outermost ring, the intensity of the rings begins to rise.

After the experimental discovery of thermal self-diffraction brought on by self-phase modulation (SPM) in the continuous waveguide laser, the relative phase shift, $\Delta\Phi$, suffered by the beam while traversing a sample of thickness was used to calculate n_2 and the thermo-optic coefficient, dn/dT, for CdSNPs films according to the following equations (AL-Ahmad et al. 2013; Badran 2015):

$$\Delta n = n_2 I \tag{19}$$

$$\Delta\Phi = \Delta n k L_{eff} \tag{20}$$

$$N = \frac{\Delta\Phi}{2\pi} \tag{21}$$

The rate at which the refractive index changes as a function of temperature (dn/dT) for NPs film is consider as a significant factor in determining the degree of such thermal effects. Because temperature has a significant impact on the thermal characteristics of CdS-NPs, different concentrations of CdS-NPs can modify their heat capacity)C_P(, density and refractive indices as a function of temperature (dn/dT) (Abdulameer et al. 2020). Therefore, it is reasonable to conclude that a change in the temperature of the CdS-NPs

Table 3 The thermal figure of merit and nonlinear parameters for CdS-NPs films

CdS-NPs temperature (°C)	N	n_2 (cm^2/W)$\times 10^{-6}$	$H \times 10^{-6}$
300	6	-0.68	1.02
400	8	-0.91	1.37
500	11	3.96	1.88

predominantly causes a change in the CdS density. The Lorentz-Lorenz relationship (Krishnamurthy and Ramalingam 2010) can be used to calculate how the index of refraction changes with density. The thermal figure of merit, H, that characterizes the CdS-NPs is given by $H = (dn/dT)(1/\rho C_P)$ (Badran et al. 2011). Thus, direct estimates of the thermal figure of merit for CdS-NPs can be obtained by measuring the thermally induced nonlinear refractive index using the thermal self-diffraction approach. According to Eqs. 19, 21 and thermal figure of meri, Table 3 lists H and n_2 values for CdS-NPs films.

6 The behavior of optical limiting

Devices called optical limiters display transmittance that is high at low intensities while aggressively attenuating optical beams at high incident intensities. Up to a predetermined intensity level, when used at low intensities, an ideal optical limiter is fully transparent. Intensity transmission is clamped at a predetermined value above that point. In order to shield the human eye and optical sensors from powerful radiation fields, these materials have vital applications. When the laser's input power is changed, the CdS-NPs output power is measured to determine the optical limitation, in the presence of an aperture. The identical laser, converging lens, sensitive photo-detector, and digital power meter utilized in Z-scan technique were also employed to measure the OL behaviors of three samples (CdS-NPs-300 °C, CdS-NPs-400 °C, CdS-NPs-500 °C). At room temperature, the experimental measurements were carried out.

Figure 17 displays the OL curve for CdS-NPs. The curve shows that, at low input power levels, the output power follows Beer's law and varies linearly with input power. With further increases in input power, the output power that is transferred starts to deviate from a linear behavior pattern and either plateaus or gets saturated. The limiting amplitude, or maximum output intensity, is the point at which the transmitted laser output-power becomes saturated. The limiting threshold (L_{th}) is a crucial concept that needs to be assessed in a material in order to assess its optical limiting property. L_{th} is the laser input-power at which transmittance reaches 50% of linear transmittance)Sheng et al. 2007; Badran and Jari 2017; Raeed et al. 2019). These findings are in line with those of the Z-scan approach, where the SDF in the CdS-NPs films is concerned. Figure 18 shows the normalized transmission (NOT) curve as a function of the incident laser power for CdS-NPs. The limiting threshold, which is the incoming laser power at which the CdS-NPs transmittance drops to half of its linear transmittance, is used to assess each sample's OL capability. Better OL performance is achieved by materials with smaller L_{th}. The optical L_{th} for the nano-particle sample are measured to be 14.6 mW, 11.5 mW, and 8.9 mW for CdS-NPs $-$300 °C, CdS-NPs-400 °C and CdS-NPs-500 °C respectively. It is abundantly obvious that the OL response of CdS-NPs at temperatures of $-$300 °C is far less robust than those of CdS-NPs-400 °C and CdS-NPs-500 °C. Additionally, it is clear that
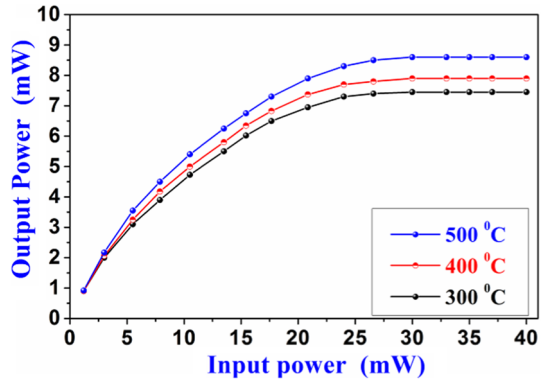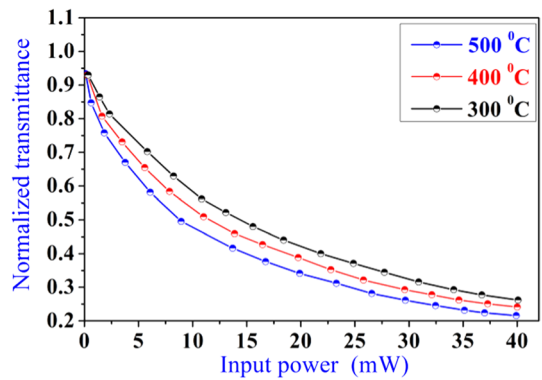
Fig. 17 Optical limiting of CdS-NPs

Fig. 18. Normalized transmission curve

CdS-NPs-500 °C, which has the biggest nonlinear refractive index of the three CdS-NPs films, exhibits the best limiting behavior. This may be attributed to the high annealing temperature and linear absorption coefficient (α_{Ab}) of CdS-NPs-500 °C at 532 nm wavelength. The α_{Ab} of CdS-NPs-300 °C is the smallest among the three CdS-NPs films, so that the threshold value is the highest possible for CdS-NPs-300 °C. The high annealing temperature and α_{Ab} of CdS-NPs-500 °C is the largest at 532 nm wavelength, so that the threshold value is the smallest. The situation of CdS-NPs-400 °C is the intermediate case. In Fig. 19, the beam spot sizes for the optical limitation presented in Fig. 17 are depicted utilizing a sensitive digital (CCD) camera with a semi-transparent screen in place of the detector for three different laser incident powers, namely 8 mW, 24 mW, and 35 mW. As input power increases, the spot size for each sample grows.

7 Mechanism for optical limiting

Numerous factors, including nonlinear absorption (reverse saturable absorption (RSA)) or two photon absorption (TPA) (Said et al. 1992) nonlinear refraction (Frobel et al. 2011), and nonlinear scattering (Nashold and Walter 1995; Nagaraja et al. 2013; Joudrier et al. 2000) can explain the OL behavior for the CdS-NPs films under study. One can refer back to the idea of NLO in order to identify the right mechanism that is accountable for or
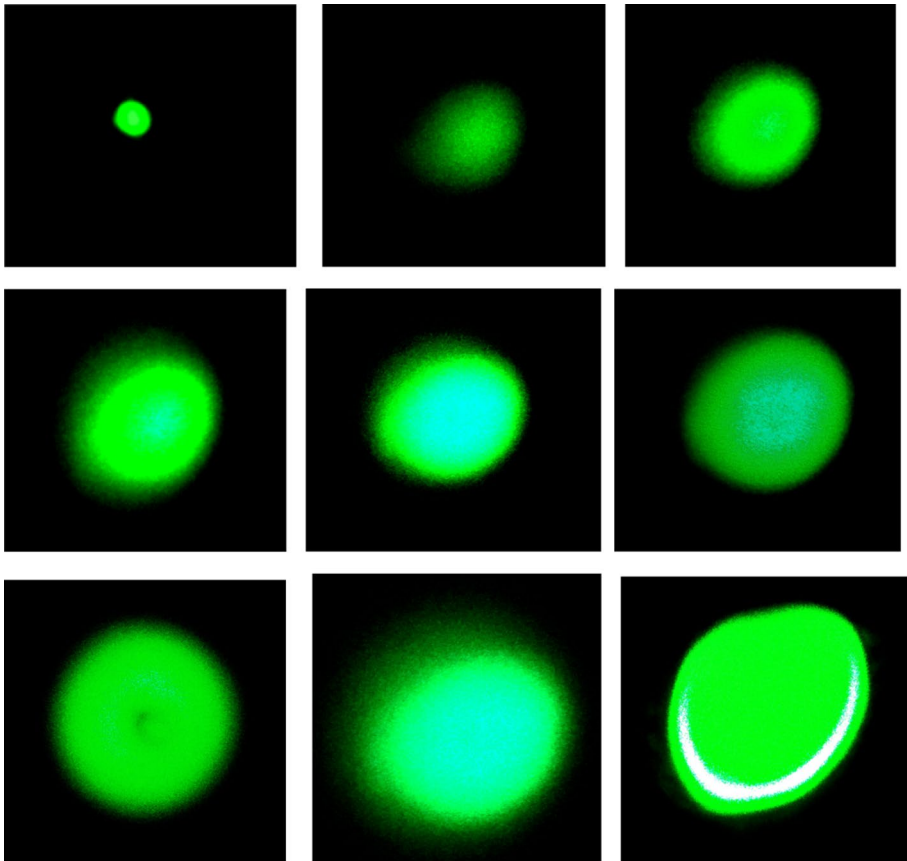
Fig. 19 Photos of the spot size as it traverses CdS-NPs **a** 300 °C, input laser powers are 8 mW **b** CdS-NPs 400 °C, input laser powers are 24 mW, and **c** CdS-NPs 500 °C, input laser powers are 35 mW

contributes to the performance limiting factor in the CdS-NPs films used in this investigation. It is well recognized that both electronic and non-electronic processes are responsible for the phenomenon of nonlinear optics (Badran 2013). The materials are promising because of the electronic nonlinearity, which arises in extremely short durations (picoseconds-nanosecond). These events, which often occur quickly on the order of picoseconds, are referred to as radiation interactions between active electrons and the optical electric field (Henari 2011). Since a CW laser was utilized in this investigation, the likelihood of reverse saturable absorption (RSA) or TPA is ruled out, and so nonlinear absorption cannot be a factor in OL. These conclusions are consistent with the current results we have obtained using the open aperture Z-scan method. Regarding the role played by nonlinear scattering in OL, no scattered radiation was observed off any of the samples at any of the various angles to the beam axis during the OL experiment. These findings show that non-linear scattering had no discernible impact on the OL trials. The nonlinear refraction may contribute significantly in nonlinear ways to the optical limitation. Temperature and other nonradiative interactions are examples of non-electronic processes that lead to nonlinear optical phenomena. These non-electronic processes have substantially longer timeframes

(such as CW laser). In the current work, a CW laser is utilized, and thermal lensing is the primary source of nonlinearity. It happens as a result of the laser beam's energy being absorbed, which heats up the medium and creates a thermal lens due to the refractive index gradient. This causes the beam to propagate in the far field with phase distortion, which results in self-defocusing. Better OL performance is obtained as a result of the material's self-defocusing, which reduces transmittance at a far field. A meaningful contribution from nonlinear refraction in the CdS-NPs films was present if there was a peak followed by a valley in the normalized transmittances in the Z-scan (self-defocusing) in Fig. 14. These findings strongly imply that the observed restriction is caused by nonlinear refraction.

8 Conclusion

In this work, Cd-SNPs were prepared on glass using a chemical reaction method. The structural and optical characteristics of CdS-NPs films deposited and annealing at different temperatures, 300 °C, 400 °C and 500 °C, were investigated. The films show that they have a hexagonal phase, in good quality, adherent and uniform. There is a good agreement between X-ray diffraction and optical results. The present CdS-NPs films show high absorbance and low transmittance in the visible region so it is possible to use them in the optoelectronics and photonic devices. The crystallization appears to get better as the film's annealing temperatures rise. It can be concluded that annealing of cadmium sulfide reduces lattice strain, producing a more perfect crystallite and decreasing the number of micro strains. The value of energy band-gap decreases from 2.5 to 2.2 eVwith increasing the annealing temperature. The extinction coefficient of the CdS films increases with increased annealing temperature while the refractive index has a sharp decrease after annealing temperature at 400°C according to the films surface begins to be oxidized at this temperature. An increase in annealing temperature appears to improve nonlinear behavior. The potential of CdS-NPs can be used in photonic and holographic devices as well as for optoelectronics devices as shown by this studying.

Declarations

approved by all named authors and that there are no other persons who satisfied the criteria for authorship but are not listed. We further confirm that the order of authors listed in the manuscript has been approved by all of us.

Consent to participate Informed consent was obtained from all authors.

Consent for publication The authors confirm that there is informed consent to the publication of the data contained in the article.

References

Abdolhossein, S., Alaa, A.A., Ahmed, S.H.: Effective role of Rb doping in controlling the crystallization, crystal imperfections, and microstructural and morphological features of ZnO-NPs synthesized by the sol–gel approach. CrystEngComm **24**, 4661–4678 (2022). https://doi.org/10.1039/d2ce00483f

Abdulameer, I., Sattar, J.B., Abdalrahman, A., Hussain, A.B.: Gamma irradiation impact on the morphology and thermal blooming of sodalime glass. AIP Conf. Proc. **2290**, 050038 (2020). https://doi.org/10.1063/5.0031473

Ahmed, S.H.: Studies on dielectric properties, opto-electrical parameters and electronic polarizability of thermally evaporated amorphous Cd50S50-xSex thin films. J. Alloys Compd. **671**, 566–578 (2016). https://doi.org/10.1016/j.jallcom.2016.02.126

Ahmed, S.H.: Intensive linear and nonlinear optical studies of thermally evaporated amorphous thin Cu–Ge–Se–Te films. J. Non-Cryst. Solids **586**, 121563 (2022). https://doi.org/10.1016/j.jnoncrysol.2022.121563

Ahmed, S.H., El Radaf, I.M.: Effect of fluorine doping on the structural, optical, and electrical properties of spray deposited Sb2O3 thin films. Mater. Sci. Semicond. Process. **160**, 107405 (2023). https://doi.org/10.1016/j.mssp.2023.107405

Ahmed, S.H., Ishu, S.: Dielectric properties, optoelectrical parameters and electronic polarizability of thermally evaporated a-Pb–Se–Ge thin films. Physica B **622**, 413330 (2021). https://doi.org/10.1016/j.physb.2021.413330

Ajeel, K.I., Kareem, Q.S.: Synthesis and characteristics of polyaniline fillid by graphene (GR) nano film. IOP Conf. J. Phys. Conf. Ser. **1234**, 012020 (2019)

Alaa, A.A., Ahmed, S.H.: Comparative microstructural studies using different methods: effect of Cd-addition on crystallography, microstructural properties, and crystal imperfections of annealed nanostructural thin CdxZn1-xSe films. Physica B **620**, 413267 (2021). https://doi.org/10.1016/j.physb.2021.413267

Alaa, A.A., El Radaf, I.M., Ahmed, S.H.: Intensive comparative study using X-Ray diffraction for investigating microstructural parameters and crystal defects of the novel nanostructural ZnGa2S4 thin films. Superlat. Microstruct. **143**, 106544 (2020). https://doi.org/10.1016/j.spmi.2020.106544

Alaa, A.A., El Radaf, I.M., Ahmed, S.H.: An extensive comparative study for microstructural properties and crystal imperfections of Novel sprayed Cu3SbSe3 Nanoparticle-thin films of different thicknesses. Optik **227**, 165837 (2021). https://doi.org/10.1016/j.ijleo.2020.165837

Al-Ahmad, A.Y., Al-Mudhaffer, M.F., Badran, H.A., Emshary, C.A.: Nonlinear optical and thermal properties of BCP:PMMA films determined by thermal self-diffraction. Opt. Laser Technol. **54**, 72–78 (2013). https://doi.org/10.1016/j.optlastec.2013.05.009

Alfahed, R.K.F., Imran, A., Majeed, M.S., Badran, H.A.: Photoluminescence characterizations and nonlinear optical of PM-355 nuclear track detector film by alpha-particles and laser irradiation. Phys. Scr. **95**, 075709–075717 (2020a). https://doi.org/10.1088/1402-4896/ab7e33

Alfahed, R.K.F., Abdulameer, I., Badran, H.A., Abdalrahman, A.: Synthesis, optical limiting behavior, thermal blooming and nonlinear studies of dye-doped polymer films. J. Mater. Sci. Mater. Electron. **31**, 13862–13873 (2020b). https://doi.org/10.1007/s10854-020-03946-y

Alfahed, R.K.F., Badran, H.A., Abutalib, Y.A., Nooralhuda, S.: Investigation of third order nonlinearity of Ethidium bromide doped deoxyribonucleic acid (DNA). J. Phys. Conf. Ser. **1963**, 012136 (2021). https://doi.org/10.1088/1742-6596/1963/1/012136

Al-Hazam, H.A., Al-fahad, R.K., Imran, A., Badran, H.A., Shaker, H.S., Alsalihi, A., Ajeel, K.I.: Preparation and optoelectronic studies of the organic compound [2-(2,3 dimethyl phenylamino)-N-phenyl benzamide doped (PMMA)]. J. Mater. Sci. Mater. Electron. **30**, 10284–10292 (2019). https://doi.org/10.1007/s10854-019-01365-2

Ali, B.: Engineering the optical properties of PVA/PVP polymeric blend in situ using tin sulfide for opto-electronics. Appl. Phys. A **126**, 335–346 (2020). https://doi.org/10.1007/s00339-020-03514-5

Ali, B.: Bandgap tuning of polyvinyl alcohol capped alloyed Sn1-xCuxS nanostructures for optoelectronic applications. J. Cryst. Growth **563**, 126091 (2021). https://doi.org/10.1016/j.jcrysgro.2021.126091

Ali, B., Sami, S.A., Althobaiti, M.G., Abdulaziz, N.A., Hasan, A., Hend, I.A., Al-Hosiny, N.: Structure investigation and optical bandgap tuning of La-doped CuO nanostructured films prepared by spray pyrolysis technique. Appl. Phys. A **127**, 235–243 (2021). https://doi.org/10.1007/s00339-021-04387-y

Ali, B., Althobaiti, M.G., Essam, E.A., Sami, S.A., Abdulaziz, N.A.: A comparative study of the structural and optical properties of transition metals (M = Fe Co, Mn, Ni) doped ZnO films deposited by spray-pyrolysis technique for optoelectronic applications. Opt. Mater. **124**, 112055 (2022a). https://doi.org/10.1016/j.optmat.2022.112055

Ali, B., Althobaiti, M.G., Sami, S.A., Abdulaziz, N.A., Ali, A.A., Sultan, E.A.: Effect of zinc doping on the structure and optical properties of iron oxide nanostructured films prepared by spray pyrolysis technique. Appl. Phys. A **128**, 123–133 (2022b). https://doi.org/10.1007/s00339-021-05154-9

Al-Salihi, A., Salim, R.D., Alfahed, R.K.F., Badran, H.A.: Effect of Solar radiation induced and alpha particles on nonlinear behavior of PM-355 film. IOP Conf. Ser. Mater. Sci. Eng. **928**, 072056 (2020). https://doi.org/10.1088/1757-899X/928/7/072056

Al-Saymari, F.A., Badran, H.A., Al-Ahmad, A.Y., Emshary, C.A.: Time dependent diffraction ring patterns in bromothymol blue dye doped PMMA film under irradiation with continuous wave green laser light. Indian J. Phys. **87**, 1153–1156 (2013). https://doi.org/10.1007/s12648-013-0334-0

Althobaiti, M.G., Sami, S.A., Abdulaziz, N.A., Ali, B.: Impact of silver/ copper dual-doping on the structure, linear and non-linear optical performance of ZnO thin films. Appl. Phys. A **128**, 539–550 (2022a). https://doi.org/10.1007/s00339-022-05682-y

Althobaiti, M.G., Abdullah, A.A., Sami, S.A., Ali, B.: Modification of the structural, linear and nonlinear optical properties of zinc oxide thin films via barium and magnesium doping. Opt. Mater. **131**, 112646 (2022b). https://doi.org/10.1016/j.optmat.2022.112646

Aziz, S.B., Rasheed, M.A., Saeed, S.R., Abdullah, OGh.: Synthesis and characterization of CdS nanoparticles grown in a polymer solution using in-situ chemical reduction technique. Int. J. Electrochem. Sci. **12**, 3263–3274 (2017)

Badran, H.A.: Z-scan measurement for the thermo-optic coefficient and transmitted beam profile of 1.8-dihydroxynaphthalin-3, 6 (disulfonic acid-[2-(4-azo)]-N-5-methyl-3-isoxazolyl)-benzene sulfonamide. Adv. Phys. Theor. Appl. **26**, 36–44 (2013)

Badran, H.A.: Thermal lens and all optical switching of new organometallic compound doped polyacrylamide gel. Results Phys. **4**, 69–72 (2014). https://doi.org/10.1016/j.rinp.2014.05.004

Badran, H.A.: Thermal properties of a new dye compound measured by thermal lens effect and Z-scan technique. Appl. Phys. B **119**, 319–326 (2015). https://doi.org/10.1007/s00340-015-6068-2

Badran, H.A., Jari, A.A.: Measurements of third-order susceptibility of 3-[[(4-methyl-1-piperazinyl) imino]-methyl]-rifamycin vs using z-scan technique. Int. Res. J. Nat. Appl. Sci. **4**, 29–38 (2017)

Badran, H.A., Hassan, Q.M.A., Al-Ahmad, A.Y., Emshary, A.: Laser-induced optical nonlinearities in Orange G, dye: polyacrylamide gel. Can. J. Phys. **89**, 1219–1224 (2011). https://doi.org/10.1139/P11-118

Badran, H.A., Al-Mudhaffer, M.F., Hassan, Q.M.A., Al-Ahmad, A.Y.: study of the linear optical properties and surface energy loss of 5',5"-dibromo-o-cresolsulfophthalein thin films. Chalcogenide Lett. **9**(12), 483–493 (2012a)

Badran, H.A., Taha, A.Y., Abdulkader, A.F., Emshary, C.A.: Preparation and study of the electrical and optical properties of a new azo dye (4-Acetaminophenol – [2-(4-Azo)]-4-Amino Dipheyl Sulfone). J. Ovonic Re. **8**, 161–170 (2012b)

Badran, H.A., Al-Ahmad, A.Y., Al-Mudhaffer, M.F., Emshary, C.A.: Nonlinear optical responses and limiting behavior of sulfadiazine-chromotropic acid azo dye. Opt. Quantum Electron. **47**, 1859–1867 (2015). https://doi.org/10.1007/s11082-014-0051-8

Badran, H.A., Hussain, H.F., Ajeel, K.I.: Nonlinear characterization of conducting polymer and electrical study for application as solar cells and its antibacterial activity. Optik **127**, 5301–5309 (2016a). https://doi.org/10.1016/j.ijleo.2016.03.030

Badran, H.A., Sultan, H.A., Qusay, M.A.H.: Surface morphology and thermal figure of merit of a new compound thin film. J. Mater. Sci. Mater. Electron. **27**, 6735–6744 (2016b). https://doi.org/10.1007/s10854-016-4622-2

Badran, H.A., Al-Fregi, A.A., Alfahed, R.K.F., Al-asadi, A.S.: Study of thermal lens technique and Third-order nonlinear susceptibility of PMMA base containing 5',5"dibromo-o cresolsulfothalein. J. Mater. Sci. Mater. Electron. **28**, 17288-17296 (2017). https://doi.org/10.1007/s10854-017-7661-4

Bokka, D., Shaik, R., Santoshi, G., Boddeti, G., Korijmella, V., Nowduri, A.: Synthesis and Characterization of Cadmium Sulphide Nanoparticles Using Annona Muricata Leaf Extract as Reducing/Capping Agent. Chem Sci Trans. **5**(4), 1035–1041 (2016)

Cheng, L., Xiang, Q., Liao, Y., Zhang, H.: CdS-based photocatalysts. Energy Environ. Sci. **11**, 1362–1391 (2018)

Chichibu, S.: Band gap energies of bulk, thin-film, and epitaxial layers of $CuInSe_2$ and $CuGaSe_2$. J. Appl. Phys. **83**, 3678 (1998). https://doi.org/10.1063/1.366588

Chikan, V.: Challenges and prospects of electronic doping of colloidal quantum dots: Case study of CdSe. J. Phys. Chem. Lett. **2**, 2783 (2011). https://doi.org/10.1021/jz2012325

Dresselhaus, M.S.: Optical Properties of Solids, Solid State Physics, Part II. University of the Pennsylvania State, State College (1998)

Eckertova, I.: Physics of Thin Films, 2nd edn. Plenum Press, New York (1986)

Fedyaeva, O.A., et al.: Optical properties research of cadmium sulphide nanoparticles received by the interaction of the reverse emulsions based on sodium bis(2-ethilhexyl)sulfosuccinate. Procedia Eng. **152**, 40–44 (2016)

Frobel, P.G.L., Suresh, S.R., Mayadevi, S., Sreeja, S., Mulkherjee, C., Muneera, C.I.: Intense low threshold nonlinear absorption and nonlinear refraction in a new organic polymer nanocomposite. Mater. Chem. Phys. **129**, 981 (2011)

Ghorbani, V., Ghanipour, M., Dorranian, D.: Effect of TiO_2/Au nanocomposite on the optical properties of PVA film. Opt. Quant. Electron. **48**, 61–73 (2016)

Ghosh, B., Pal, R.R., Mukhopadhyay, S.: An all-optical integrated system for implementing arithmetic operation in 2's complement method with the active participation of non-linear material based switches. Indian J. Phys. **84**, 1101–1109 (2010). https://doi.org/10.1007/s12648-010-0105-0

Gutierrez, R., et al.: Optical and structural properties of $CdS:Pb^{2+}$ nanocrystals. Rev. Mex. Fis. **61**, 312–322 (2015)

He, X.W., Liu, W.F., Zhu, Ch.F., Jiang, G.S.: CdS thin films deposited by CBD method on glass. Chin. J. Chem. Phys. **24**, 471 (2011). https://doi.org/10.1088/1674-0068/24/04/471-476

Henari, F.: Nonlinear characterization and optical switching in bromophenol blue solutions. Nat. Sci. **3**, 728–732 (2011)

Hussain, B.A., Abd-AL-Aladil, K., Lazim, H.G., Al-Ahmad, A.Y.: Thermal blooming and photoluminescence characterizations of sol–gel $CdO–SiO_2$ with different nanocomposite. J. Mater. Sci. Mater. Electron. **27**, 2012–2220 (2016a). https://doi.org/10.1007/s10854-015-4013-0

Hussain, A.B., Ajeel, K.I., Lazim, H.G.: Effect of nano particle sizes on the third-order optical nonlinearities and nanostructure of copolymer P3HT:BCPM thin film for organic photovoltaics. Mater. Res. Bull. **76**, 422–430 (2016b). https://doi.org/10.1016/j.materresbull.2016.01.005

Hussain, A.B., Ahmed, A., Alfahed, R.K.F., Bahjat, A.S., Al-Ahmad, A.Y., Al-Saymari, F.A., Rita, S.E.: Synthesis, surface profile, nonlinear reflective index and photophysical properties of curcumin compound. J. Mater. Sci. Mater. Electron. **29**, 10890–10903 (2018). https://doi.org/10.1007/s10854-018-9167-0

Hussain, A.B., Al-Hazam, H.A., Al-Fahad, R.K., Ajeel, K.I.: Second-order hyperpolarizability and nonlinear optical properties of novel organic compound doped Poly(O-methoxyaniline) polymer film. J. Mater. Mater. Electron. **32**, 14623–14641 (2021). https://doi.org/10.1007/s10854-021-06021-2

Hussain, A.B., Abu Talib, Y.A., Alfahed, R.K.F.: Study the effect of concentration on the evolution of far-field diffraction patterns of Bromocresol purple and Congo red solution. J. Phys. Conf. Ser. **1963**, 012013 (2021). https://doi.org/10.1088/1742-6596/1963/1/012013

Joudrier, V., Bourdon, P., Hache, F., Flytzanis, C.: Characterization of nonlinear scattering in colloidal suspensions of silica particles. Appl. Phys. B **70**, 105–109 (2000)

Kadem, B., Alfahed, R.K.F., Al-Asadi, A.S., Badran, H.A.: Morphological, structural, optical and photovoltaic cell of copolymer P3HT: ICBA and P3HTPCBM. Optik **204**, 164153 (2020). https://doi.org/10.1016/j.ijleo.2019.164153

Kale, R.B., Lokhand, C.D.: Influence of air annealing on the structural, morphological, optical and electrical properties of chemically deposited ZnSe thin films. Appl. Surf. Sci. **252**, 929–938 (2005). https://doi.org/10.1016/j.apsusc.2005.01.154

Kathirvel, P., Manoharan, D., Mohan, S.M., Kumar, S.: Spectral investigations of chemical bath deposited zinc oxide thin films—ammonia gas sensor. J. Optoelectron. Biomed. Mater. **1**(1), 25–33 (2009)

Ketam, A.A., Hussain, A.B.: Nonlinear optical properties and diffraction ring patterns of benzo congo red. Eur. J. Appl. Eng. Sci. Res. **1**, 66–72 (2012)

Krishnamurthy, R.R., Ramalingam, A.: Nonlinear characterization of Mercurochrome dye for potential application in optical limiting. Opt. Appl. **XL**(1), 187 (2010)

Lazim, H.G., Ajeel-Khalid, I., Badran, H.A.: The photovoltaic efficiency of the fabrication of copolymer P3HT:PCBM on different thickness nano-anatase titania as solar cell. Spectrochim. Acta Part A Mol. Biomol. Spectrosc. **145**, 598–603 (2015). https://doi.org/10.1016/j.saa.2015.02.096

Lee, J.: Comparison of CdS films deposited by different techniques: effects on CdTe solar cell. Appl. Surf. Sci. **252**(5), 1398–1403 (2005). https://doi.org/10.1016/j.apsusc.2005.02.110

Lee, H.L., Issam, A.M., Belmahi, M., Assouar, M.B., Rinnert, H., Alnot, M.: Synthesis and characterizations of bare CdS nanocrystals using chemical precipitation method for photoluminescence application. J. Nanomater. **2009**, 914501 (2009)

Mahawela, P., Jeedigunta, S., Vakkalanka, S., Ferekides, C.S., Morel, D.L.: Transparent high-performance CDSE thin-film solar cells. Thin Solid Films **480**, 466–470 (2005). https://doi.org/10.1016/j.tsf.2004.11.066

Mahdi, M.A., Kasem, S.J., Hassen, J.J., Swadi, A.A., Al-Ani, S.K.J.: Structural and optical properties of chemical deposition CdS thin films. Int. J. Nanoelectron. Mater. **2**(2), 41–52 (2009)

Mahdi, M.A., Hassan, Z., Ng, S.S., Hassan, J.J., MohdBakhori, S.K.: Structural and optical properties of nanocrystalline CdS thin films prepared using microwave-assisted chemical bath deposition. Thin Solid Films **520**, 3477–3484 (2012)

Mahesh Kamble, M., et al.: Optical, structural and morphological study of CdS nanoparticles: role of sulfur source. Nanomater. Energy **9**(1), 72–81 (2020)

Manickathai, K., Kasi Viswanathan, S., Alagar, M.: Synthesis and characterization of CdO and CdS nanoparticles. Indian J. Pure Appl. Phys. **46**, 551–564 (2008)

Moss, T.S.: Optical Properties of Semiconductors. Academic Press, New York (1974)

Nagaraja, K.K., Pramoddini, S., Santhoshkumar, A., Nagaraja, H.S., Poornesh, P., Kekuda, D.: Third-order nonlinear optical properties of Mn doped ZnO thin films under CW laser illumination. Opt. Mater. **35**, 431–439 (2013)

Nashold, K.M., Walter, D.P.: Investigations of optical limiting mechanisms in carbon particle suspensions and fullerene solutions. J. Opt. Soc. Am. B **12**, 1228–1237 (1995)

Ogusu, K., Kohtani, Y., Shao, H.: Laser-induced diffraction rings from an absorbing solution. Opt. Rev. **3**, 232–234 (1996). https://doi.org/10.1007/s10043-996-0232-1

Pankove, J.I.: Optical Processes in Semiconductors. Prentice-Hall, New York (1971)

Pantoja, E.J.: Effect of annealing time and temperature on structural, Optical and Electrical Properties of Cds Films Deposited by Cbd. Chalcogenide Lett. **10**(2), 45–53 (2013)

Qi, L.M., Ma, J.M., Cheng, H.M., Zhao, Z.G.: Synthesis and characterization of mixed CdS-ZnS nanoparticles in reverse micelles. Colloids Surf., A **111**, 195–2025 (1996)

Raeed, F.K.A., Al-Asadi, A.S., Badran, H.A., Ajeel, K.I.: Structural, morphological, and Z-scan technique for a temperature-controllable chemical reaction synthesis of zinc sulfide nanoparticles. Appl. Phys. B **125**, 48–58 (2019). https://doi.org/10.1007/s00340-019-7154-7

Ramteke, G.G., Lanje, A.S.: Synthesis and characterization of CdS nanoparticles by chemical precipitation method. Int. J. Res. Biosci. Agric. Technol. IJRBAT **12**(2), 68–71 (2017)

Ramteke, G.G., Lanje, A.S., Pimpalshende, D.M.: Effect of CU^{2+} doping on structural and optical properties of CdS nanoparticles. Int. J. Curr. Eng. Sci. Res. IJCESR **5**(5), 11–17 (2018)

Rathore, A., Nagar, A., Malav, S., Kumar, M.R.: Synthesis of CdS nanoparticles by precipitation method and antibacterial activities. Int. J. Adv. Res. Sci. Eng. **6**(10), 819–825 (2017)

Said, A.A., et al.: Determination of bound-electronic and free-carrier nonlinearities in ZnSe, GaAs, CdTe, and ZnTe. J. Opt. Soc. Am. B **9**, 405–414 (1992)

Saravanan, L., Diwakar, S., Mohankumar, R., Pandurangan, A., Jayavel, R.: Synthesis, structural and optical properties of PVP encapsulated CdS nanoparticles. Nanomater. Nanotechnol. **1**(2), 42–48 (2011)

Sheik-Bahae, M., Said, A.A., VanStryland, E.W.: High-sensitivity single beam n_2 measurements. Opt. Lett. **14**, 955 (1989)

Sheng, L.G., Tie, P.L., Tie, B.W., Zhao, S.L., Tian, D.C.: Third-order nonlinearities and optical limiting properties of complex CO_2L_3. Opt. Mater. **29**, 494–498 (2007)

Shinde, P.S., Adhav, L.D., Pise, R.M., Jagtap, S.S.: Synthesis and characteristics of CdS nanoparticles in normal (1g) and simulated microgravity (SMG). Buletin Fisika **22**(1), 7–11 (2021)

Srinivasa, R.B., Rajesh Kumar, B., Rajagobal Reddy, V., Rao, S.: preparation and characterization of CdS nanoparticles by chemical co-precipitation technique. Chalcogenide Lett. **8**(3), 177–185 (2011)

Tezuka, K., Takagi, H., Shan, Y.J., Imoto, H.: Simple synthesis of zinc sulfide and cadmium sulfide under hydrothermal conditions. J. Ceram. Soc. Jpn. **119**, 55–59 (2011)

Ullrich, B., Bagnall, D.M., Sakai, H., Segawa, Y.: Photoluminescence and lasing of thin CdS films on glass formed by pulsed-laser-deposition. J. Lumin. **87–89**, 1162–1164 (2000)

Yang, F., et al.: The morphology-property effect and synergetic catalytic effect of CdS as electro catalysts for dye-sensitized solar cells. ECS J. Solid State Sci. Technol. **7**(6), 311–316 (2018)

Ziadan, K.M., Hussein, H.F., Ajeel, K.I.: Study of the electrical characteristics of poly(O-tolidine) and application in Solar cell. Energy Procedia **18**, 157–164 (2012)

Authors and Affiliations

Harith A. Hasan[1] · Nadia A. Hussein Al-Assady[2] · Hussain A. Badran[3] · Raeed K. Alfahed[4] · Khalid I. Ajeel[3]

> Harith A. Hasan
> harth.alqata100@yahoo.com

> Nadia A. Hussein Al-Assady
> nadia.hussain@uobasrah.edu.iq

> Raeed K. Alfahed
> rrr80kkk@yahoo.com

> Khalid I. Ajeel
> drkiajeel2013@yahoo.com

[1] Department of Material Science, Polymer Research Centre, University of Basrah, Basrah, Iraq

[2] Department of Chemistry, College of Education for Pure Sciences, University of Basrah, Basrah, Iraq

[3] Department of Physics, College of Education for Pure Sciences, University of Basrah, Basrah, Iraq

[4] Al-Nahrain Renewable Energy Research Center, Al-Nahrain University, Jadriya, Baghdad, Iraq